92PC92104-TPR-16

ADVANCED THERMALLY STABLE JET FUELS

Technical Progress Report
April - June 1996

H.H. Schobert, S. Eser, C. Song, P.G. Hatcher, A. Boehman, M.M. Coleman

Contributions from:

Jian Yu, Prashant Sanghani, and Andrew Schmitz

November 1996

Prepared for U.S. Department of Energy
under
Contract No. DE-FG22-92PC92104

DISCLAIMER

TABLE OF CONTENTS

OBJECTIVES

The Penn State program in advanced thermally stable jet fuels has five components: 1) development of mechanisms of degradation and solids formation; 2) quantitative measurement of growth of sub-micrometer and micrometer-sized particles during thermal stressing; 3) characterization of carbonaceous deposits by various instrumental and microscopic methods; 4) elucidation of the role of additives in retarding the formation of carbonaceous solids; and 5) assessment of the potential of producing high yields of cycloalkanes and hydroaromatics from coal.

SUMMARY

The thermal decomposition of *n*-butylcyclohexane was studied in the near-critical and the supercritical regions, in 45–50 mL Pyrex glass tube reactors. At the highest conversion achieved, 39% (at 475 °C, 20 minutes) about 130 compounds were formed as reaction products. The reaction is initiated by homolytic cleavage of a carbon-carbon bond. A variety of reactions account for formation of secondary products. Differences in yields of products can be explained by differences in relative formation rates of parent radicals and in rates of subsequent decomposition reactions.

Work continued on the development of a kinetic model for deposit formation from jet fuel. In the present reporting period, work focused on parameter estimation from multi-response data. Zeolite-supported Pt and Pd catalysts were prepared using a mordenite (HM38) and a Y-zeolite (HY) as support materials, and were applied for hydrogenation of naphthalene in n-tridecane at 200°C in the absence and presence of added benzothiophene. The results are also compared to those with Al_2O_3- and TiO_2-supported Pt and Pd catalysts. Both Pd/HM38 and Pd/HY catalysts are substantially more active than Pd/Al_2O_3 and Pd/TiO_2 catalysts, even when the former is used with less catalyst loading under lower H_2 pressure. The same trend can be observed from comparing Pt/HM38 and Pt/HY catalysts with Pt/Al_2O_3 and Pt/TiO_2 catalysts. The sulfur-resistance as well as the activity of the catalysts also depends strongly on the type of support and metal. Addition of sulfur in the form of benzothiophene decreased the activity of all the catalysts tested. However, there appear to be significant improvements in sulfur tolerance of the noble metals when they are supported on zeolites, rather than Al_2O_3 or TiO_2 supports. The Pd catalysts supported on both Y zeolite and mordenite showed higher sulfur tolerance than all the other

catalysts. Overall, Pd/HM38 catalyst showed the best activity and the highest resistance to sulfur poisoning.

Task 1. Investigation of the Quantitative Degradation Chemistry of Jet Fuels

Thermal Decomposition of n-Butylcyclohexane in Near-Critical and Supercritical Regions: Product Distributions and Reaction Mechanisms (Contributed by Jian Yu and Semih Eser)

Introduction

Jet fuels contain significant amounts of alkylcyclohexanes. For example, JP-8P, a petroleum-derived jet fuel, and JP-8C, a coal-derived jet fuel, contain about 14 wt% and 40 wt% of C_6 to C_{14} cyclohexanes, respectively [1]. Therefore, studying thermal decomposition of alkylcyclohexanes is important for understanding thermal degradation behavior of jet fuels.

In this work, thermal decomposition of *n*-butylcyclohexane was studied in near-critical and supercritical regions. Thermal stressing experiments were carried out in a Pyrex glass tube reactor with a total volume of 45–50 mL.

Results and Discussion

1. Product Distributions. The liquid products from thermal decomposition of *n*-butylcyclohexane include cyclohexane, methylenecyclohexane, cyclohexene, methylcyclohexane, vinylcyclohexane, allylcyclohexane, ethylcyclohexane, 1-methylcyclohexene, 3-methylcyclohexene, methylcyclopentane, 1-ethylcyclohexene, *n*-propylcyclohexane, C_4-cyclohexenes, and C_4-cyclohexanes. Among these compounds, the first seven are the primary products. Some high-molecular-weight compounds, although not identified, were also found as the conversion exceeds 10%. At the highest conversion (39%, 475 °C, 20 min), about 130 peaks were obtained from the chromatogram of the liquid products.

Figure 1 shows the product distributions as a function of initial reduced pressure for the thermal decomposition of *n*-butylcyclohexane at 425 °C for 15 min. The initial reduced pressure ($P_r = P/P_c$) was calculated at the given temperature and loading ratio, defined as the sample volume at room temperature divided by the reactor volume, using Soave-Redlich-Kwong equation of state [2]. The conversion steadily decreases from 3.24 to 1.82% as P_r increases from 0.67 to 2.64, as shown in Figure 2. It can be seen from Figure 1 that the yields of the primary products decrease while those of the secondary products, except methylcyclopentane, increase as pressure increases, indicating the increasing importance of the secondary reactions with the increasing pressure. Under supercritical conditions, the most abundant liquid products are 1-methylcyclohexene and cyclohexane, followed by cyclohexene, methylcyclohexane, and vinylcyclohexane. Other liquid products are present in lower yields (< 5 mol/100 mol reactant converted). The 1-methylcyclohexene and 3-methylcyclohexene seem

to be converted from methylenecyclohexane because the total yield of these three compounds remains almost unchanged (32.4±1.5 mol/100 mol reactant converted) within the pressure range examined.

Figure 3 shows the product distributions as a function of the conversion for the thermal decomposition of *n*-butylcyclohexane at 450 °C with a loading ratio of 0.36 (P_r = 1.71). The relationship between the conversion and reaction time is shown in Figure 4. It can be seen from Figure 3 that the yields of the saturated compounds (cyclohexane, methylcyclohexane, ethylcyclohexane, *n*-propylcyclohexane, and methylcyclopentane) remain unchanged with the increasing conversion, indicating higher stabilities of these compounds. Among the unsaturated compounds, the yields of 1-methylcyclohexene, vinylcyclohexane, and allylcyclohexane decrease while those of methylenecyclohexane and cyclohexene do not change significantly with the increasing conversion. The yield of 3-methylcyclohexene first increases and then remains at a stable level and that of 1-ethylcyclohexene increases and then decreases as the conversion increases.

2. Reaction Mechanisms. The reaction products from thermal decomposition of *n*-butylcyclohexane can be divided into those from primary reactions and those from secondary reactions. Eqs 1 to 8 show the major primary reactions:

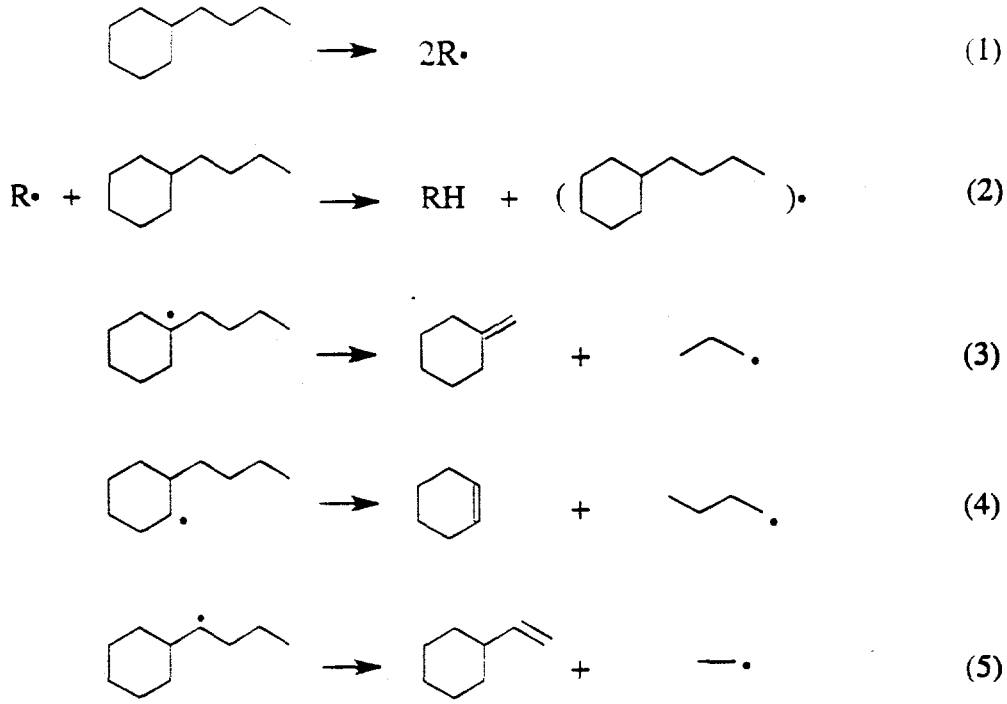

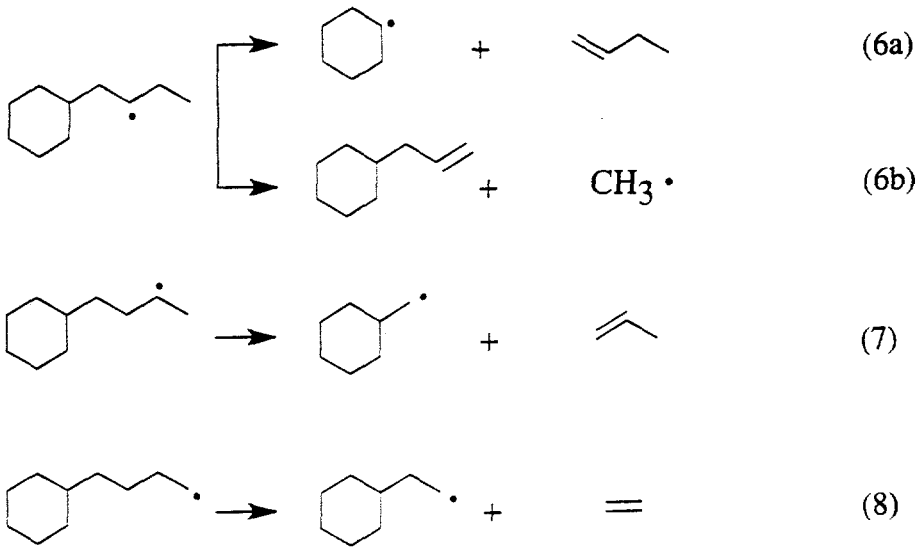

(6a)

(6b)

(7)

(8)

The initiation occurs by homolytic cleavage of carbon-carbon bond to produce two radicals (eq 1). These radicals then abstract hydrogen atoms from the surrounding *n*-butylcyclohexane molecules to form various parent radicals (eq 2). Each of these parent radicals could decompose by β-scission to form a small radical and an unsaturated product (eqs 3-8). The formation of methylenecyclohexane, cyclohexane, cyclohexene, methylcyclohexane, vinylcyclohexane, allylcyclohexane, and ethylcyclohexane can be explained by these primary reactions.

The secondary products can be produced by the following reactions:

(9)

(10)

(11)

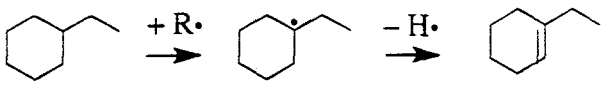

(12)

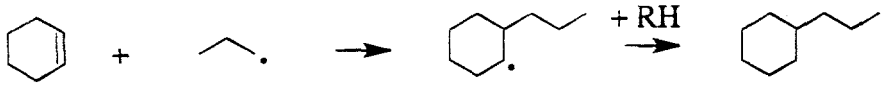

(13)

Methylenecyclohexane could be converted to 1-methylcyclohexene by the reactions shown in eq 9. This conversion should be fast because the abstraction of a secondary allylic hydrogen on the ring of methylenecyclohexane is a relatively easy process. The 1-methylcyclohexene could be converted to 3-methylcyclohexene by similar reactions, as shown in eq 10. Methylcyclopentane could be formed by β-scission of the cyclohexyl radical, followed by ring closure and subsequent hydrogen abstraction (eq 11). The 1-ethylcyclohexene could be formed from ethylcyclohexane by the reactions shown in eq 12. The *n*-propylcyclohexane could be produced from the addition of 1-propyl radical to cyclohexene, followed by hydrogen abstraction (eq 13).

The differences in the yields of individual reaction products can be explained by the differences in the relative formation rates of the parent radicals and differences in the subsequent decomposition rates of these radicals. Among the various parent radicals, the formation of a tertiary butylcyclohexane radical (the left hand side of eq 3) would be favored because of its relatively higher stability as compared with other parent radicals (secondary or primary). One would expect the yield of methylenecyclohexane to be highest among the primary products. Examination of Figures 1 and 3 reveals that this is not the case. This is because methylenecyclohexane is rapidly converted to 1-methylcyclohexene, as discussed before. It seems that high-pressure supercritical conditions favor this conversion, as shown in Figure 1.

The rates for the formation of α-, β-, and γ-butylcyclohexane radicals should be equivalent because of the similar dissociation energies of secondary carbon-hydrogen bonds. One would expect the yields of vinylcyclohexane, cyclohexane plus allylcyclohexane, and methylcyclohexane to be roughly equal. Examination of Figures 1 and 3 reveals that the yield of cyclohexane is much higher than those of vinylcyclohexane and methylcyclohexane. This difference in product yield can be attributed to the difference in the decomposition rate for the three parent radicals. The decomposition of the β-butylcyclohexane radical by β-scission on C_{ring}–C_α bond would be favored because a relatively stable secondary cyclohexyl radical is produced. The decomposition of other two radicals produces less stable primary radicals. Therefore, cyclohexane would be formed in higher yield than vinylcyclohexane and methylcyclohexane. It should be noted that the decomposition of the β-butylcyclohexane radical could also occur by β-scission on C_γ–C_δ bond. However, this route for β-scission is much less favorable because the methyl radical is highly unstable. This can be confirmed by the low yield of allylcyclohexane.

The yield of vinylcyclohexane is equivalent to that of methylcyclohexane at low pressures but decreases as pressure increases, indicating that the significant addition reaction

occurs between a radical and this compound. The yield of cyclohexene is higher than those of vinylcyclohexane and methylcyclohexane because the concentration of butylcyclohexyl radical (the left hand side of eq 4) is higher than those of α- and γ-butylcyclohexane radicals. Ethylcyclohexane is formed in a low yield because the formation of a primary butylcyclohexane radical is less favorable.

References

1. Schobert, H. H.; Eser, S.; Boehman, A.; Song, C.; Hatcher, P. G.; Coleman, M. M. Advanced Thermally Stable Jet Fuels, Technical Progress Report (April 1995 – June 1995), August 1995, The Pennsylvania State University.
2. Soave, G. Chem. Eng. Sci. 1972. 27. 1197-1203.

Task 2 Investigation of Incipient Deposition

Deposit Growth During Heating of Coal-Derived Aviation Gas Turbine Fuels (Contributed by Prashant C. Sanghani and André L. Boehman)

This work is a continuation of the development of a kinetic model for deposit formation from complex hydrocarbon mixtures such as jet fuel. Development of a kinetic model requires rate parameter estimation from multi-response data. Parameter estimation from multi-response data has been reported previously [1,2].

Parameter estimation from experimental data is considered as the inverse problem of a dynamic model. This can be described as a system of ordinary differential equations (ODE):

$$dC/dt = f(t, C, \theta) \qquad (1)$$

where C is a vector of concentration variables, t is reaction time. θ is the vector of parameters (e.g. rate coefficients), and f are the functions representing species mass balance. One is given the initial conditions of $C = C_0$ and asked to find the parameter values, θ, such that solution of Eq. 1

$$C = g(\theta.t.\ C_0) \qquad (2)$$

matches the experimental data. $C = C^{obs}$. Mathematically this is stated as a minimization of an objective function ϕ with respect to the parameters θ, where ϕ is expressed as:

$$\phi(\theta) = \sum_{i=1}^{n} \omega_i [\, C_i^{obs} - C(\theta) \,]^2 \qquad (3)$$

where n is the number of experimental observations and ω_i is the weighting factor of i th observation.

Optimization of (3) can be done by a search algorithm in a multidimensional space θ with a call to a differential equation solver each time new values of parameters θ are evaluated. When the number of parameters to be estimated is small, this method works well. This was verified by solving an example problem involving ODEs with four unknown parameters which are to be determined from experimental data. The differential equation solver coupled with the optimization routine efficiently solved the problem with a small number of parameters.

However, when the number of parameters to be estimated increases (greater than 12), this method fails [3] because extremely large numbers of function evaluations are required, which places large demand on computation time.

To overcome this difficulty a method of solution mapping was proposed [3]. In this work, the method of solution mapping will be used for kinetic parameter estimation. In this technique, C in eq. (2) is approximated by simple algebraic expressions, i.e.

$$g(\theta, C_0) = \Psi(\theta) \qquad (4)$$

in the subspace Ω of parameter space θ. The approximating functions $\Psi(\theta)$ are obtained by means of computer experiments known as factorial design [4]. The computer experiments are performed using the complete kinetic model.

On substituting Eq. (4) into Eq. (3), we obtain

$$\phi(\theta) = \sum_{i=1}^{n} \omega_i [C_i^{obs} - \Psi_i(\theta)]^2. \qquad (5)$$

This means optimization of the objective function no longer requires time consuming numerical integration of differential equations but rather straight forward evaluations of $\Psi(\theta)$. That is, this method decouples the ODE solver from the optimization search.

As an illustration, consider the following problem of parameter estimation from chemical kinetics where k1, k2, k3 and kd need to be determined from experimental values of F, H1, H2, and D :

dF/dt = k1 * (F)

dR/dt = k1 * (F) - k2 * (H1) * (R) - k3 * (H2) * (R) - kd * (R)

dH1/dt = -k2 * (H1) * (R)

dH2/dt = -k3 * (H2) * (R)

dD/dt = kd * R

where F, H1, H2, D represent different species taking part in the reactions. Also values of F, H1, H2, D at time t, where t = t1, t2, t3 ...., are known.

1. Specify the ranges of rate parameters k(1), k(2), k(3) and k(d) as

ln[k1] = ln[k(1,0)] +/- ln[delta(1)]

ln[k2] = ln[k(2,0)] +/- ln[delta(2)]

ln[k3] = ln[k(3,0)] +/- ln[delta(3)]

ln[kd] = ln[k(d,0)] +/- ln[delta(d)]

where k(i,0) is the initial guess of the i th rate parameter, and delta(i) is a positive value and is the (arbitrarily) assigned range of rate parameter k(i). Let

X(i) = ln[k(i)/k(i,0)] / ln [delta(i)]

where X(i) is a factorial variable, such that

X(i) = 1 for k(i) = k(i,0) * delta(i)

X(i) = 0 for k(i) = k(i,0)

X(i) = -1 for k(i) = k(i,0) / delta(i)

2. Make a 2^2 factorial design [4] of X(i), i.e.,

J	X(1)	X(2)	X(3)	X(d)
1	+1	+1	+1	+1
2	+1	+1	+1	-1
3	+1	+1	-1	+1
4	+1	+1	-1	-1
5	+1	-1	+1	+1
6	+1	-1	+1	-1
7	+1	-1	-1	+1
8	+1	-1	-1	-1
9	-1	+1	+1	+1
10	-1	+1	+1	-1
11	-1	+1	-1	+1
12	-1	+1	-1	-1
13	-1	-1	+1	+1
14	-1	-1	+1	-1
15	-1	-1	-1	+1
16	-1	-1	-1	-1
17	0	0	0	0

Compute the responses, i.e., F(t), H1(t), H2(t) and D(t), at each design point j (j=1,J) for every time t1, t2, t3 .... at which experimental values of F, H1, H2, and D are available. After calculating values for the responses , one will have a table which looks like

J X(1) X(2) X(3) X(d) F(t1) F(t2) .. H1(t1), H1(t2) .. H2(t1) etc.
1 +1 +1 +1 +1 F11 F12 .. H111 H112 .. H211 etc.
2 +1 +1 +1 -1 F21 F22 .. H121 H122 .. H212 etc.
3 +1 +1 -1 +1
4 +1 +1 -1 -1 .....
5 +1 -1 +1 +1 .....
6 +1 -1 +1 -1
7 +1 -1 -1 +1
8 +1 -1 -1 -1
9 -1 +1 +1 +1
10 -1 +1 +1 -1
11 -1 +1 -1 +1
12 -1 +1 -1 -1
13 -1 -1 +1 +1
14 -1 -1 +1 -1
15 -1 -1 -1 +1
16 -1 -1 -1 -1
17 0 0 0 0

Using linear regression, one can then obtain a second-order polynomial for each of the responses, e.g.,

ln[F(t1, polynomial)] = aF0 + aF1 X(1) + aF2 X(2) + aF3 X(3)
+ aF4 X(4) + aF11 X(1)^2 + aF12 X(1)*X(2)
+ .....

where the aF's are polynomial parameters. In essence, the above exercise gives the numerical dependence of F, H1, H2 and D on k(i). Because F, H1, H2 and D depend only on k(i) and not on t, costly integration of the ODE system for each optimization search is not required.

3. Optimization: Minimize

$$L^2 = \sum_j [F(tj,polynomial) - F(tj,expt)]^2 + \sum_j [H1(tj,polynomial) - H1(tj,expt)]^2 + \sum_j [H2(tj,polynomial) - H2(tj,expt)]^2 + \sum_j [D(tj,polynomial) - D(tj,expt)]^2$$

with respect to k(1), k(2), k(3) and k(d), where F(tj,polynomial) etc. is the developed polynomial and F(tj,expt) is the experimental value at time tj.

This new method will be used in our problem of kinetic model development.

References

1. Ziegel E. R. and Gorman J. W.; Technometrics, vol. 22, No. 2, 1980, 139-151.
2. Stewart W. E., Caracotsios M., and Sorensen J. P.; AIChe Journal, vol. 38, No. 5, 1992.
3. Frenklach M., Wang H. and Rabinowitz M. J.; Prog. Energy Combust. Sci., vol. 18, 1992, pp. 47-73.
4. Box G. E. P., Hunter W. G. and Hunter J. S.; Statistics for Experimenters, An Introduction to Design, Data Analysis, and Model Building, Wiley, New York (1978).

Task 5. Exploratory Studies on the Direct Conversion of Coal to High-Quality Jet Fuels

Zeolite-Supported Pd and Pt Catalysts for Low-Temperature Hydrogenation of Naphthalene in the Absence and Presence of Benzothiophene (contributed by Chunshan Song and Andrew D. Schmitz)

Introduction

This work is concerned with low-temperature hydrotreating for reduction of aromatics in jet fuels. Hydrogenation of aromatic compounds is typically exothermic, and is therefore thermodynamically favored at a lower reaction temperature. However, in conventional hydrotreating processes, a reaction temperature above 350°C is typical, which consequently results in relatively higher contents of aromatics at equilibrium composition. Deep hydrogenation of aromatics requires a higher concentration of hydrogen to offset the limitation of thermodynamic equilibrium conversion at high temperatures. Conventional supported Ni-Mo and Co-Mo sulfided catalysts become active only at relatively high temperatures.

Hydrogenation of the two-ring aromatics in coal-derived liquids can produce thermally stable decalin and methyldecalin components. In addition, due to increasingly more stringent environmental regulations and fuel specifications, deep reduction of aromatics in distillate fuels has received considerable attention. Noble metal catalysts are active for the hydrogenation of aromatics, even below 200°C, but they are not used for hydrotreating owing to higher cost and susceptibility to poisoning by sulfur-containing compounds. However, recent studies have shown that some noble metal catalysts may not be as sensitive to sulfur as previously thought (Stanislaus and Cooper, 1994).

This study aimed at examining the potential of zeolite-supported Pd and Pt catalysts for low-temperature hydrotreating of distillate fuels in the absence and presence of benzothiophene. Hydrogenation of naphthalene in *n*-tridecane was chosen as a model reaction for fuel hydrotreating. The zeolite supports mordenite and Y were selected because they are distinctly different from conventional supports such as alumina and titania, and may offer several advantages. This work is a part of our on-going effort to develop advanced thermally stable jet fuels from coal-derived liquids and petroleum, where both complete and partial hydrogenation reactions of naphthalene-type compounds are important. Complete saturation of naphthalene gives decalins which show much higher thermal stability than long-chain alkanes (Song et al., 1993),

while partial saturation produces tetralin which can substantially inhibit the thermal degradation and solid-forming tendency of long-chain alkanes in jet fuels at high temperature (Song et al., 1994).

Experimental

Catalyst Preparation. Zeolite-supported Pt and Pd catalysts were prepared from the NH_4-form of a synthetic mordenite (HM38) and the NH_4-form of a synthetic Y-zeolite (HY) supports (see Table 1, used as received), by incipient wetness impregnation of either aqueous $H_2PtCl_6xH_2O$ (Aldrich, 99.995% Pt, metal basis) or $PdCl_2$ (Aldrich, 99.999% Pd, metal basis) dissolved in dilute hydrochloric acid (sufficient to form soluble $PdCl_4^{2-}$) to a nominal metal concentration of 2 wt%. Following drying in vacuo, the catalysts were calcined in air at 450°C for 2 h. Metal reduction was done in situ during naphthalene hydrogenation tests under the high-pressure of hydrogen. The preparation procedure for Al_2O_3- and TiO_2-supported Pt and Pd catalysts has been described elsewhere (Lin and Song, 1996).

Catalyst Evaluation. Catalyst tests were done at 200°C for 2 h (unless otherwise mentioned) in a 30 cm^3 stainless-steel microautoclave reactor. The reactor system is tee-shaped with most of the internal volume in the horizontal tube that contains the catalyst and reactants. The horizontal section is connected by a 10" length of 1/4" o.d. tubing to a pressure gauge and valve. Unless otherwise specified, the reactor was charged with 0.1 g catalyst, 1.0 g (7.8 mmol) naphthalene (Aldrich, 99%), 4.0 g *n*-tridecane solvent, and 0.35 g *n*-nonane internal standard. Benzothiophene was added in controlled amounts for runs with sulfur. The charged reactor was flushed with H_2, then pressurized to 1000 psig H_2 (cold) to start the test. Naphthalene can undergo hydrogenation, even at room temperature, so a consistent procedure was established to minimize the time between reactor pressurization and the start of the run. The reactor was mounted on a holder and immersed in a fluidized sand bath heater. Mixing was accomplished by vertically agitating the reactor at 240 min^{-1}, with a 1 cm stroke.

At the end of the test, the reaction was quenched by immersing the reactor in cold water. After cooling, the gas headspace was collected for analysis and the reactor was opened. The contents of the reactor were then washed with acetone onto a filter, and the solid was dried for XRD examination. Solution products were analyzed by GC-MS and GC-FID. For both GC instruments, the column was 30mx0.25mm DB-17 (J&W Scientific), and the oven temperature program was 100-280°C at 15°C/min. GC

and GC-MS indicate that cracking or isomerization of *n*-tridecane and *n*-nonane, if any, were negligible under the conditions used. The yields of products were determined by quantitative GC analysis using n-nonane as internal standard, and the conversion was determined by the amount of naphthalene recovered after the reaction.

Results and Discussion

Table 2 gives the properties of the laboratory-prepared Pd and Pt catalysts supported on zeolites. The total surface areas of the two Pd catalysts, 2% Pd/HY and 2% Pd/HM38, are almost identical. However, the latter possess more surface area in mesopore range but the former more surface area in micropore range. Similarly, 2% Pt/HY catalyst has larger surface area enclosed in micropore range, but 2% Pt/HM38 catalyst has more surface area in mesopore range.

Table 3 shows the results for hydrogenation of naphthalene in n-tridecane at 200°C over 2% Pd/HY and 2% Pd/HM38 catalysts. Both catalysts display high activity for complete hydrogenation of naphthalene to form decalin. For the purpose of performance evaluation, Figure 5 compares the present data on zeolite-supported Pd catalysts with our previous data with 2% Pd/Al_2O_3 and 2% Pd/TiO_2 catalysts obtained under comparable conditions (Lin and Song, 1996). Both Pd/HM38 and Pd/HY catalysts are substantially more active than Pd/Al_2O_3 and Pd/TiO_2 catalysts, even when the former is used with less amount of catalyst under lower H_2 pressure.

Table 4 gives the results for naphthalene hydrogenation on Pt/HM38 and Pt/HY obtained in this work. Figure 6 compares the present results with those from recent work in this laboratory using Pt/Al_2O_3 (Lin and Song, 1996). The Pt/HM38 catalyst appears to be more active than the Pt/HY and Pt/ Al_2O_3 catalyst. Comparing Pt and Pd catalysts, Pt catalysts often gives higher selectivity to *cis*-decalin, while Pd catalysts afford higher selectivity to *trans*-decalin. We have shown in our previous work that *cis*-decalin isomerizes into *trans*-decalin over some zeolite catalysts (Song and Moffatt, 1994), and this conformational isomerization proceeds more readily over some zeolite-supported Pd and Pt catalysts (Lai and Song, 1996). It can be seen from Tables 3 and 4 that the best selectivities to *trans*- and *cis*-decalin are observed with Pd/HM38 and Pt/HY, respectively. These results are consistent with those observed in related work using 6% Pd and 6% Pt catalysts supported on zeolites (Schmitz et al., 1996).

Since sulfur tolerance is an important aspect of practical application of the proposed low-temperature hydrogenation, we also examined the effect of sulfur addition on the low-temperature catalytic activity and selectivity of the catalysts.

Although the fuels should have been desulfurized prior to the hydrogenation over noble metal catalysts, trace amounts of sulfur in the feedstocks are inevitable in industrial practice. We have designed a series of accelerated sulfur tolerance tests in which excess benzothiophene was added so that the sulfur to noble metal atomic ratio is above 1. The amount of sulfur added is large enough to cover all the metal particles even if they are ideally dispersed at the molecular level.

Table 3 also presents the comparative data for the sulfur tolerance tests of Pd catalysts. Addition of sulfur in the form of benzothiophene decreased the activity of all the catalysts tested. However, there appear to be significant improvements in sulfur tolerance of the noble metals when they are supported on zeolites, rather than Al_2O_3 or TiO_2 supports. As can be seen from Figure 3, the order of apparent catalytic conversion of naphthalene in the presence of benzothiophene appears to be Pd/HM38 > Pd/HY > Pd/TiO_2 > Pd/Al_2O_3. The data on the sulfur tolerance tests of Pt catalysts are given in Table 4. The most significant drawback of the Pt catalysts for fuel hydrotreating applications is their very low sulfur tolerance. Supporting Pt on zeolites does not appear to improve the sulfur tolerance as compared to that of Pt supported on alumina. At S/Pt ratio of about 8, the naphthalene conversion drops to such a low level ($\leq$ 10%) with all the Pt catalysts that their use for treating sulfur-containing fuels does not seem to be practically applicable. It should be mentioned that an impregnation method was used for preparing the Pt and Pd catalysts in this work, and it remains to be clarified whether the observed trends apply to the catalysts obtained by other methods.

The higher sulfur tolerance of the zeolite-supported Pd catalysts relative to the Al_2O_3-supported one may be related to the electron deficiency of the noble metal (Stanislaus and Cooper, 1994). Dalla Betta and Boudart (1972) first introduced the term "electron deficiency" to account for higher hydrogenation activity of Pt in Y zeolite. This term refers to the electron transfer from noble metal to the zeolite.

Figures 8 and 9 show naphthalene conversion and product selectivity for hydrogenation at 200°C for 2 h using 0.1–0.2 g Pd/HM38 and Pd/HY catalysts, respectively, as a function of the S/Pd atomic ratio. Figure 5 indicates that naphthalene conversion decreases with increasing S/Pd atomic ratio above 1.8, and tetralin becomes the main product when S/Pd atomic ratio is above 1.8. These results indicate that naphthalene hydrogenation can still proceed over Pd/HM38 catalyst in the presence of added sulfur, even when the S/Pd ratio is above 9. Sulfur addition passivates almost all the active sites for hydrogenation of tetralin.

It is worth noting that naphthalene conversion does not change when the S/Pd ratio is increased from 0 to 1.8 in the case of Pd/HM38, while hydrogenation of tetralin is nearly completely inhibited at S/Pd ratio of 1.8. An important implication is that partial passivation of the Pd/HM catalyst by addition of an appropriate amount of sulfur can lead to nearly complete hydrogenation of naphthalene with over 95% selectivity to partially hydrogenated product, tetralin. Earlier work in this laboratory has shown that addition of tetralin can significantly improve the thermal stability of aviation jet fuels at high temperatures (Song et al., 1994).

Figure 9 indicates that the activity of Pd/HY catalyst decreases rapidly with increasing sulfur addition, up to S/Pd ratio of about 3. Similar to the case of Pd/HM38, sulfur addition passivates the sites for hydrogenation of tetralin. It is apparent by comparing Figure 8 with Figure 9 that Pd/HM38 has significantly higher sulfur tolerance than Pd/HY under otherwise identical conditions. Some industrial hydrocracking catalysts are prepared by supporting noble metal on Y-zeolite. The present results suggest that a partially dealuminated mordenite such as HM38 may be a more attractive support than Y-zeolite for preparing sulfur-resistant hydrogenation catalysts and hydrocracking catalysts.

It is very interesting to note that both the activity and the sulfur tolerance of the zeolite-supported noble metal catalysts depend on the type of support and metal. Mordenite-supported Pd and Pt catalysts are more active than Y zeolite-supported Pd and Pt, respectively, although the mordenite has lower surface area than the Y-zeolite (Table 1). One possible explanation is that Pd is better dispersed in mordenite pore structure. Mordenite-supported Pd exhibits higher sulfur tolerance than the Y zeolite-supported Pd. On the other hand, the Pt catalysts loaded on both types of zeolites have very low sulfur tolerance.

HM38 and HY have significantly different structures. Mordenite has a channel-like pore structure in which the basic building blocks consist of five-membered rings; the mordenite pore structure consists of elliptical, noninterconnected channels. The major channels are circumscribed by 12-membered oxygen rings, which have major and minor diameters of 7.0 and 6.7 Å, respectively (Bhatia, 1990). Side pockets that open off the main channel have a free diameter of 3.9 Å (Bhatia, 1990). The faujasite-type zeolites X and Y have a network of three-dimensional intersecting channels in which the minimum free diameter is the same in each direction. These zeolites consist of an array of cavities having internal diameters of about 12 Å; access to each cavity (supercage) is through six equispaced necks having a diameter of about 7.4 Å formed by a ring comprising 12 oxygen atoms (Satterfield, 1991). The pore diameters of both

mordenite and Y zeolite are large enough to admit naphthalene (Satterfield, 1991; Gates, 1992).

Judging from the results in Tables 2 and 3 and Figures 5 and 6, sulfur tolerance under hydrogenation conditions may be divided into two types: tolerance to organosulfur compounds (I) and to hydrogen sulfide (II). Type I tolerance may be improved partly by preventing the access of sulfur to the metal. This may be partially achieved if the metal atom can be dispersed into the side-pockets in mordenite (Hypothesis **A**). It has been reported by Sachtler et al. that Pt atoms are located in the side-pockets of the main channel in Pt/mordenite (Lerner et al., 1992; Sachtler and Zhange, 1993). If this is also achieved for Pd, molecular H_2 can dissociate on the metal inside the side-pocket channel, but the chemisorption of large-sized organosulfur compounds is difficult on the metal located in the side pocket channel (Hypothesis **B**). The hydrogen atoms generated dissociatively on the metal atom can spillover to the main channel to promote hydrogenation and the hydrodesulfurization of the adsorbed sulfur molecules. Hydrodesulfurization produces H_2S, which is sufficiently small compared to any fuel molecules in the feedstock, and may diffuse into the side-pocket of the dealuminated mordenite at the reaction temperature (Hypothesis **C**). Type II tolerance can not be improved easily by taking advantage of pore structure of zeolites.

To gain some insight into the reactions that organosulfur compounds may undergo over the zeolite-supported Pd and Pt catalysts, we have also quantified the products attributable to benzothiophene. Table 4 shows the conversion of benzothiophene and seletivities to ethylbenzene, ethylcyclohexane, and dihydrobenzothiophene. It should be mentioned that the mass balance for these analytical data is below 90% in most cases, because the absolute amount of the added sulfur compound is only 8–21 mg and the recovery of unreacted benzothiophene may not be complete. Nonetheless, some important information has been derived from these analyses, which partially supports the above hypothetical discussions.

As shown in Table 5, first of all, when Pd/HM38 is used with the S/Pd ratios below 4.1, most of the benzothiophene is converted by hydrodesulfurization reactions to ethylbenzene and ethylcyclohexane, and only a small amount remains as dihydrobenzothiophene. This means that Pd/HM38 has hydrodesulfurization ability, although it is passivated by benzothiophene. In the case of Pt/HM38 and Pt/HY, the dominant product is dihydrobenzothiophene, which can still strongly adsorb on the Pt catalysts. At high level of sulfur addition with S/Pd ratios of 7.9-9.9, the distribution of products and benzothiophene conversions over Pd/HM38 and Pd/HY are similar to those over Pt/HM38 and Pt/HY, respectively. The amounts of H_2S formed are

therefore similar, but the former still shows much higher naphthalene conversion. This comparison suggests that Pd has higher type II sulfur tolerance than Pt when supported on the same material. It is likely that Pt catalysts have low type I and type II sulfur tolerance, which accounts for the experimental observations.

Summarizing the industrially important observations from Table 2, the Pd catalysts supported on both mordenite and Y zeolite showed higher sulfur tolerance than all the other catalysts for naphthalene hydrogenation. Overall, Pd/HM38 catalyst showed the best activity and the highest resistance to sulfur poisoning. Clarification of the mechanism of improved sulfur tolerance is needed in future work.

Conclusions

In noble-metal catalyzed hydrogenation of aromatics in distillate fuels, the activity, selectivity and sulfur-resistance of the catalysts strongly depends on the type of support and metal.

For hydrogenation of naphthalene in *n*-tridecane at 200°C in the absence of added sulfur, Pd/HM38 and Pd/HY catalysts are substantially more active than Pd/Al_2O_3 and Pd/TiO_2 catalysts, even when the former is used with less amount of catalyst under lower H_2 pressure. Pt/HM38 catalyst shows higher activity than Pt/HY and Pt/Al_2O_3 catalysts.

Mordenite-supported Pd and Pt catalysts are more active than Y zeolite-supported Pd and Pt, respectively. At 100% conversion, Y zeolite-supported catalysts afford higher yield of *cis*-decalin, while mordenite-supported catalysts give higher yield of *trans*-decalin.

Addition of sulfur in the form of benzothiophene decreased the activity of all the catalysts tested. However, there appear to be significant improvements in sulfur tolerance of the noble metals when they are supported on zeolites, rather than Al_2O_3 or TiO_2 supports. The Pd catalysts supported on both Y zeolite and mordenite showed higher sulfur tolerance than all the other catalysts.

Overall, Pd/HM38 catalyst showed the best activity for naphthalene hydrogenation and the highest resistance to sulfur poisoning. On the other hand, the Pt catalysts loaded on zeolites or alumina have very low sulfur tolerance. The mordenite-supported Pd catalyst is promising for practical application and therefore warrants further study.

References

Bhatia, S. *Zeolite Catalysis: Principals and Applications.* CRC Press, Boca Raton, Florida, 1990, Chapter 2.

Dalla Betta, R. A. and Boudart, M. Proc. 5th Int. Congr. Catal., 1972, p.1329.

Gates, B. C. *Catalytic Chemistry.* Wiley & Sons, New York, 1992, Chapter 5.

Lai, W.-C., and Song, C. Catalysis Today, 1996, in press.

Lerner, B. A., Carvill, B. T., and Sachtler, W. M. H. J. Mol. Catal., 1992, 77, 99.

Lin, S.D., and Song, C. Catalysis Today, 1996, in press.

Poondi, D. and Vannice, M.A. J. Catal., 1996, 161, 742.

Sachtler, W. M. H. and Zhange, Z. Adv. Catal., 1993, 39, 129.

Satterfield, C. N. *Heterogeneous Catalysis in Industrial Practice.* 2nd Ed., McGraw-Hill, New York, 1991, Chapter 7.

Schmitz, A., Bowers, G. and Song, C. Catalysis Today, 1996, in press.

Song, C., Eser, S., Schobert, H. H. and Hatcher. P. G. Energy & Fuels, 1993, 7, 234.

Song, C. and Moffatt, K. Microporous Materials. Elsevier, 1994, 2, 459.

Song, C., Lai, W.-C. and Schobert, H. H. Ind. Eng. Chem. Res., 1994, 33, 548.

Stanislaus, A. and Cooper, B. H. Catal. Rev. - Sci. Eng., 1994, 36, 75.

Table 1. Properties of the Supports and Their Nominal Properties

Support ID	Material Type	Surface Area, m^2/g	Pore Vol cc/g	SiO_2/Al_2O_3 mol ratio	Na_2O wt%	Supplier and Code
HY	Y zeolite	948	0.3	5.0	2.5	Linde, LZ-Y62
HM38	Mordenite	512	0.3	37.5	0.07	PQ, CBV 30A
Al_2O_3	γ-Alumina	200	0.8			Sumitomo Metal, S-1
TiO_2	Titania	50	0.5			Degussa, P-25

Table 2. Properties of the Laboratory-Prepared Pd and Pt Catalysts Supported on Zeolites

Catalyst ID	Support Zeolite Type	Metal Loading wt%	Tot. Pore Vol cc/g	Tot. Surface Area m^2/g	Micropore Area m^2/g	Mesopore Area m^2/g
Pd/HY	Y zeolite	1.88 wt% PdO	0.296	538.0	529.6	8.4
Pd/HM38	Mordenite	1.97 wt% PdO	0.351	539.4	356.4	183.0
Pt/HY	Y zeolite	1.97 wt% PtO_2	0.370	589.3	562.9	26.4
Pt/HM38	Mordenite	1.86 wt% PtO_2	0.368	541.6	363.4	178.2

Table 3. Comparison of Zeolite-Supported Pd Catalysts with Al_2O_3- and TiO_2-Supported Catalysts at 200°C.

Expt ID	225	244	245	226	227	246	247	SL#A	112#1	115#1	117#1	SL#B	112#3	115#3	117#3
Metal, 2 wt%	Pd	Pd	Pd	Pd	Pd	Pd	Pd	Pd	Pd	Pd	Pd	Pd	Pd	Pd	Pd
Support	HM38	HM38	HM38	HY	HY	HY	HY	Al_2O_3	Al_2O_3	Al_2O_3	Al_2O_3	TiO_2	TiO_2	TiO_2	TiO_2
Catalyst mass, mg	100	200	201	102	101	201	200	135	208	198	195	138	214	197	194
H_2 pressure, psig	1000	1500	1500	1000	1000	1500	1500	1500	1500	1500	1500	1500	1500	1500	1500
Naph, mg	1001	1000	1000	1001	1000	1000	1000	1002	1004	1001	1002	1002	1002	1002	1001
Reaction time, h	2	2	2	1	2	2	2	2	2	2	2	2	2	2	2
Benzothiophene, mg	0	9.0	20.8	0	0	9.8	21.8	0	0	9	21	0	0	9	21
Sulfur in feed, ppm		405	934			441	976			429	998		0	429	999
S/Metal, atom ratio		1.8	4.1			1.9	4.3			1.8	4.3		0	1.8	4.3
Naph Conv (%)	100	100	75.8	100	100	61.0	34.0	42	100	47	16	37	100	61	43
Prod Sel (mol %)															
Tetralin	0	91.1	97.2	0.4	0	98.7	98.8	98	39	99.2	91.5	97	0.6	99.1	98.4
cis-Decalin	6.7	3.8	1.1	58.0	55.0	0.3	0.2	tr.	17	tr.	tr.	tr.	19	tr.	0.1
trans-Decalin	92.4	4.3	1.1	40.0	43.1	0.5	0.2	tr.	44	0.6	tr.	0.4	81	0.4	0.4
Other	0.9	0.9	0.6	1.6	1.9	0.5	0.9								

Table 4. Comparison of Zeolite-Supported Pt Catalysts with Al_2O_3-Supported Catalysts at 200°C for 1-2 h.

Expt ID	220	221	228	222	223	230	SL#C	112#2	115#2	117#2
Metal	Pt	Pt	Pt	Pt	Pt	Pt	Pt	Pt	Pt	Pt
Support Type	HM38	HM38	HM38	HY	HY	HY	Al_2O_3	Al_2O_3	Al_2O_3	Al_2O_3
Catalyst mass, mg	100	100	100	102	1000	100	124	207	191	184
H_2 pressure, psig	1000	1000	1000	1000	1000	1000	1500	1500	1500	1500
Naph, mg	1000	1001	1000	1000	1001	1001	1001	1004	1003	1004
Reaction time, hour	1	2	2	1	2	2	2	2	2	2
Benzothiophene, mg	0	0	11.4	0	0	10.9	0	0	9	21
Sulfur in feed, ppm			500			489			429	998
S/Metal, atom ratio			8.3			7.9			3.3	7.8
Naph Conv (%)	100	100	2.1	96.5	100	2.4	11	100	13	10
Prod Sel (%)										
Tetralin	0	0	58.1	86.6	1.6	86.5	90	0.7	99	74
cis-Decalin	40.3	29.9	13.9	10.7	72.0	5.4	tr.	53	0	0
trans-Decalin	58.4	68.8	8.1	2.3	24.4	3.0	tr.	47	0	0
Other	1.3	1.3	15.3	0.4	2.0	5.1				

Table 5. Products Attributable to the Reactions of Added Benzothiophene (BTP) over Zeolite-Supported Catalysts at 200°C for 2 h.

Expt ID	225	232	233	244	245	227	234	235	246	247	221	228	229	223	230	231
Metal, 2 wt%	Pd	Pd	Pd	Pd	Pd	Pd	Pd	Pd	Pd	Pd	Pt	Pt	Pt	Pt	Pt	Pt
Support	HM38	HM38	HM38	HM38	HM38	HY	HY	HY	HY	HY	HM38	HM38	HM38	HY	HY	HY
Cat mass, mg	100	100	100	200	201	101	100	100	201	200	100	100	100	100	100	100
H_2 P, psig	1000	1000	1000	1500	1500	1000	1000	1000	1500	1500	1000	1000	1000	1000	1000	1000
Naph, mg	1001	1000	1000	1000	1000	1000	1000	1000	1000	1000	1001	1000	1001	1001	1001	1001
BTP, mg	0	8.3	24.9	9.0	20.8	0	8.3	24.4	9.8	21.8	0	11.4	20.0	0	10.9	19.3
S in feed, ppm		373	1098	405	934		373	1095	441	976		500	895		489	850
S/M atom ratio		3.3	9.9	1.8	4.1		3.3	9.7	1.9	4.3		8.3	14.5		7.9	14.0
BTP Conv (%)	na	100	91.9	96.8	100	na	88.2	81.2	93.6	85.4	na	93.3	83.4	na	71.5	71.1
Mass Balance	na	100	78.3	83.8	72.9	na	77.8	76.8	51.4	46.0	na	71.9	79.7	na	90.0	69.6
Prod Sel (%)																
Et-cyclohexane	0	36.1	11.6	13.5	7.4	0	25.3	6.4	5.5	2.3	0	17.6	7.5	0	22.1	13.5
Et-benzene	0	63.9	36.0	80.5	71.9	0	26.8	18.9	73.0	48.5	0	25.9	13.5	0	4.9	3.8
Dihydro-BTP	0	0	52.4	6.0	20.7	0	48.0	74.7	21.5	49.2	0	56.5	79.0	0	73.0	82.7

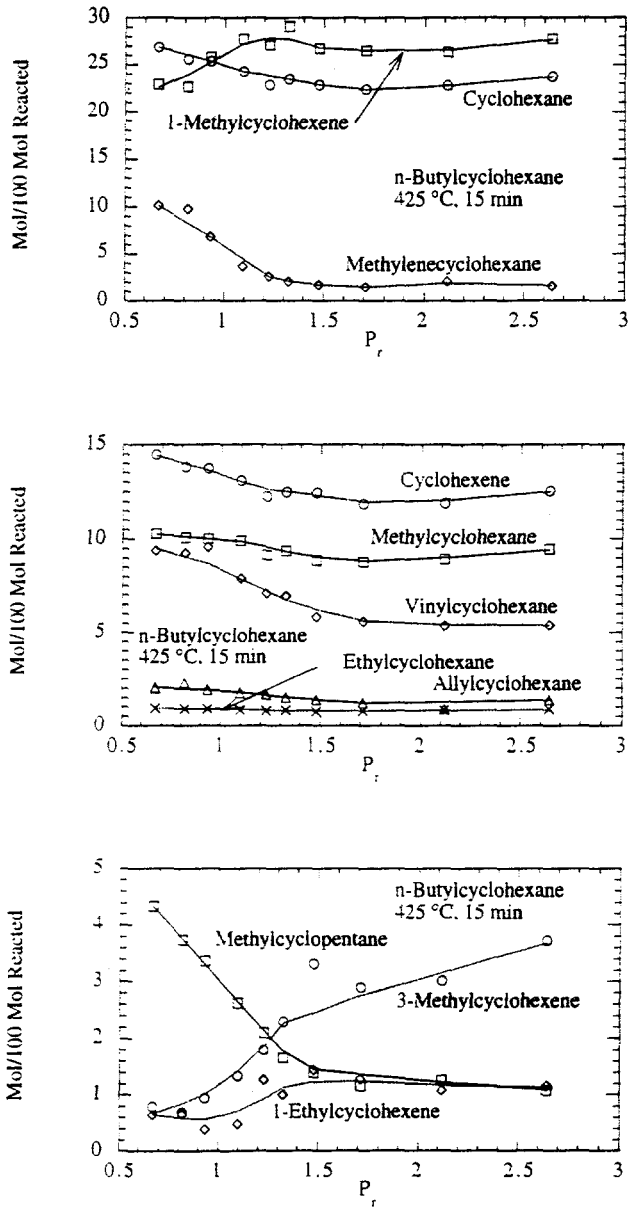

Figure 1. Product Distributions as a Function of Initial Reduced Pressure for Thermal Decomposition of *n*-Butylcyclohexane.

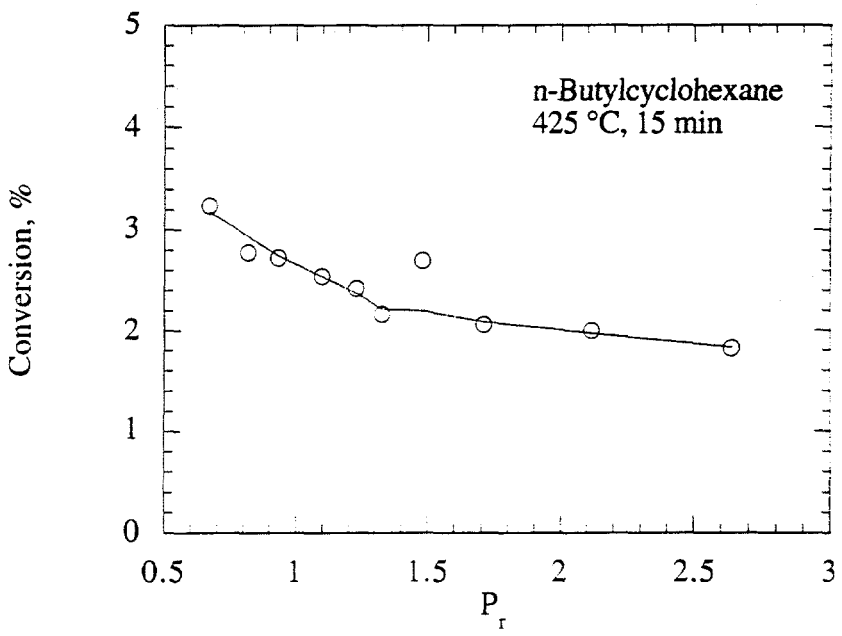

Figure 2. Conversion as a Function of Initial Reduced Pressure

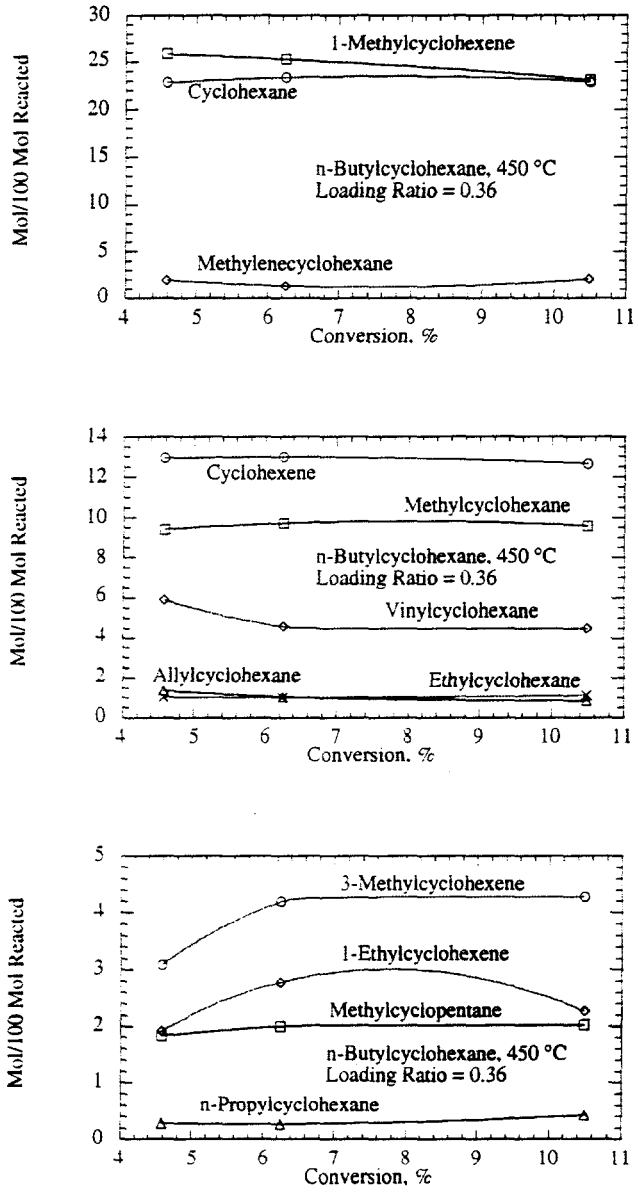

Figure 3. Product Distributions as a Function of Conversion for Thermal Decomposition of *n*-Butylcyclohexane.

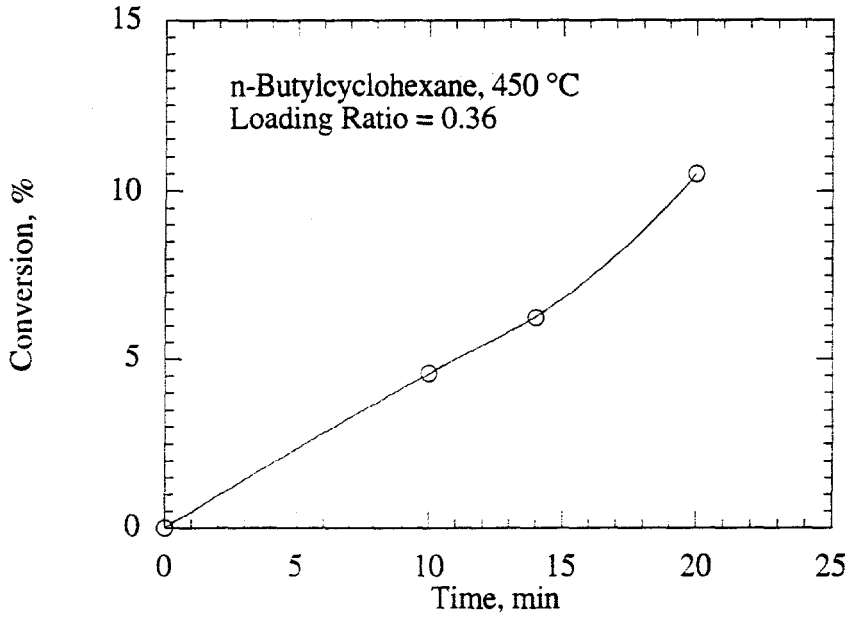

Figure 4. Conversion as a Function of Reaction Time

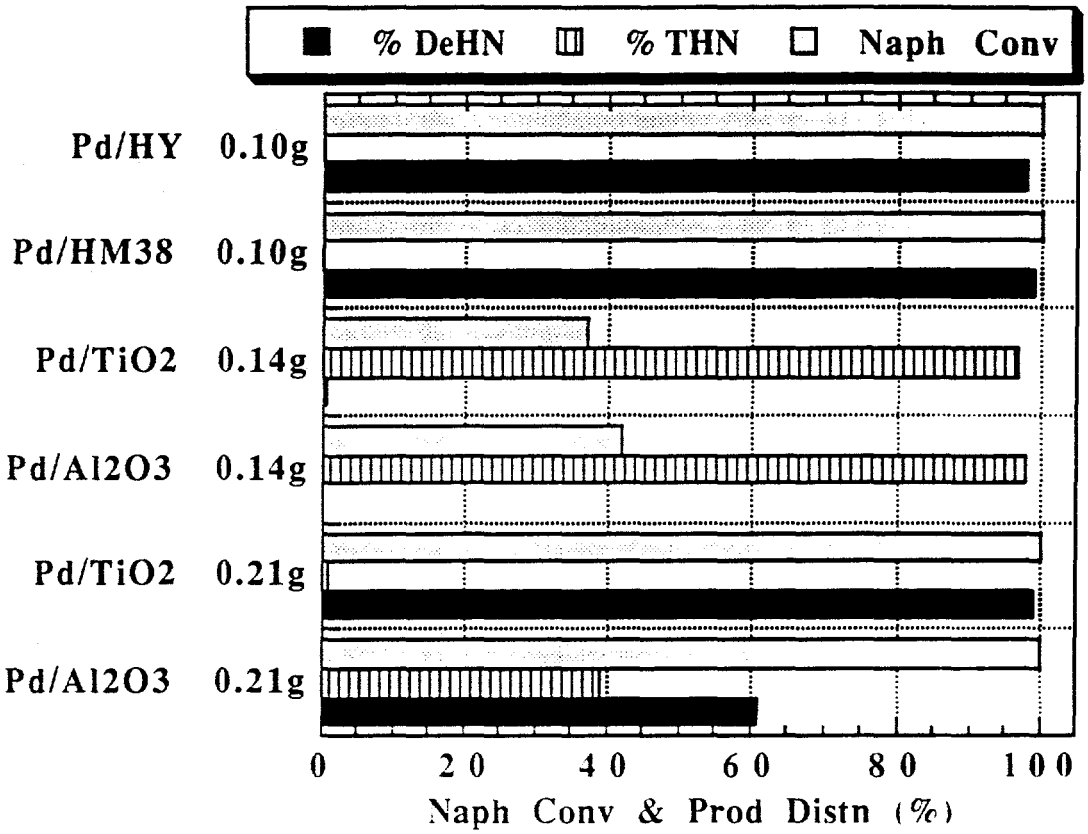

Figure 1. Naphthalene hydrogenation using in situ reduced Pd catalysts at 200°C for 2 h under 1000 psig H_2 (PdHY and Pd/HM38) or 1500 psig H_2 (Pd/Al_2O_3, Pd/TiO_2).

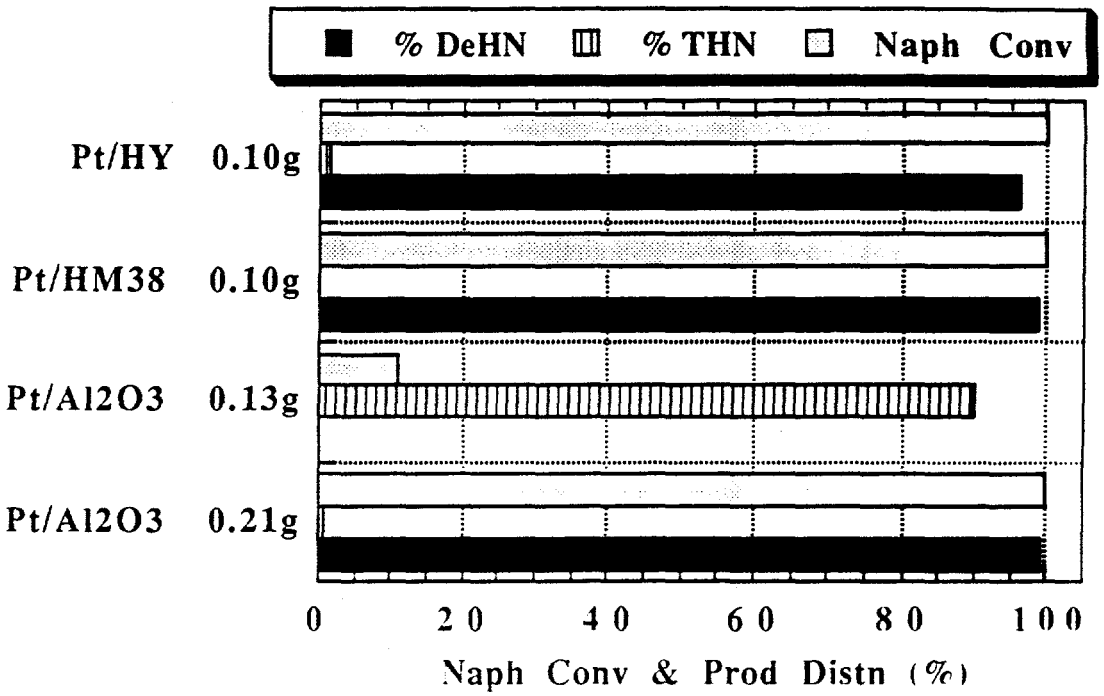

Figure 2. Naphthalene hydrogenation using in situ reduced Pt catalysts at 200°C for 2 h under 1000 psig H_2 (Pt/HY and Pt/HM38) or 1500 psig H_2 (Pt/Al_2O_3).

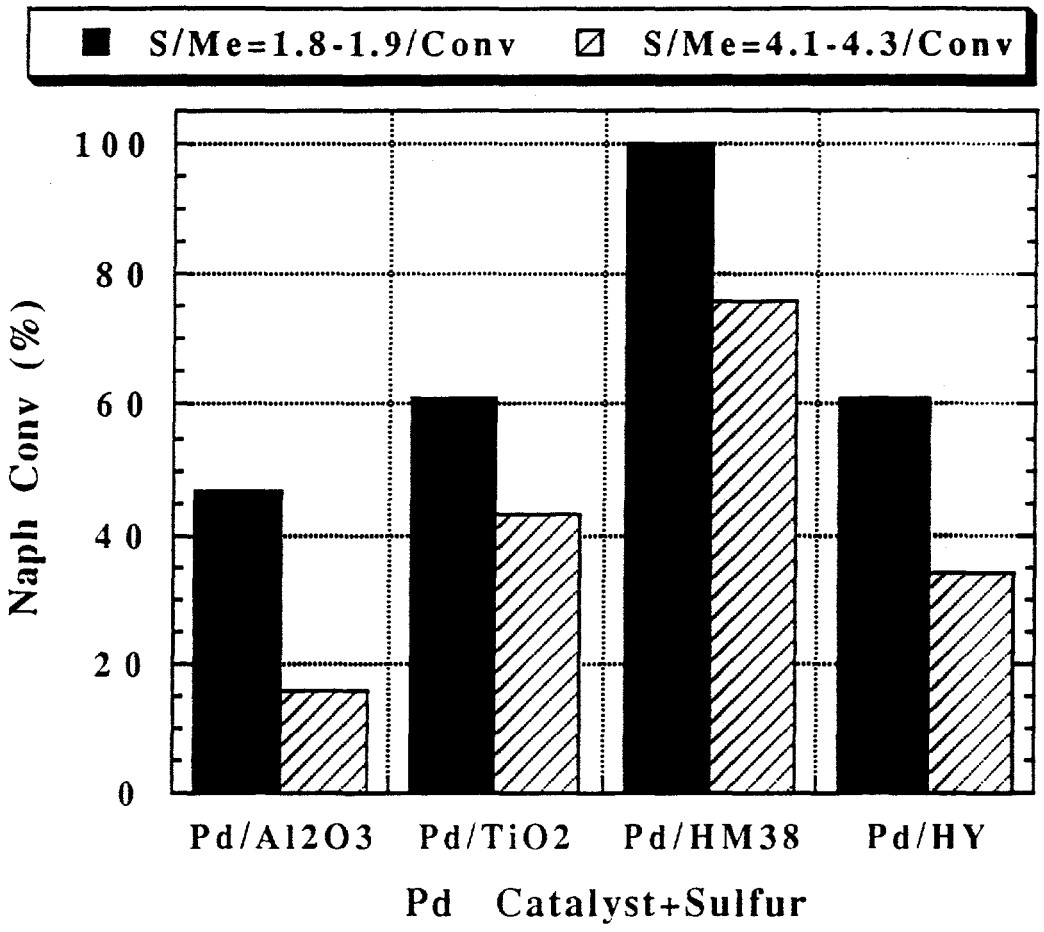

Figure 3. Comparison of sulfur tolerance of various Pd catalysts in the presence of benzothiophene at 200°C for 2 h under 1500 psig H_2. The atomic ratios of sulfur to Pd ranges from 1.8 to 4.3.

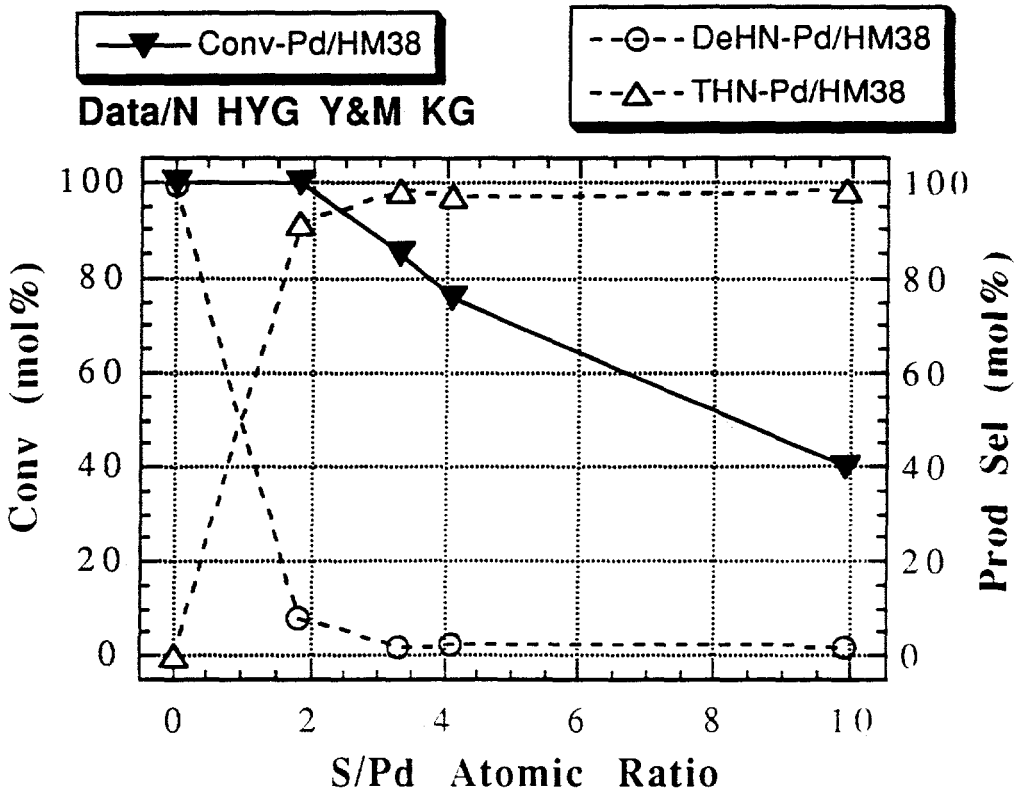

Figure 4. Effect of sulfur/Pd atomic ratio on naphthalene conversion and selectivity to tetralin and decahydronaphthalene over Pd/HM38 at 200°C in the presence of added benzothiophene.

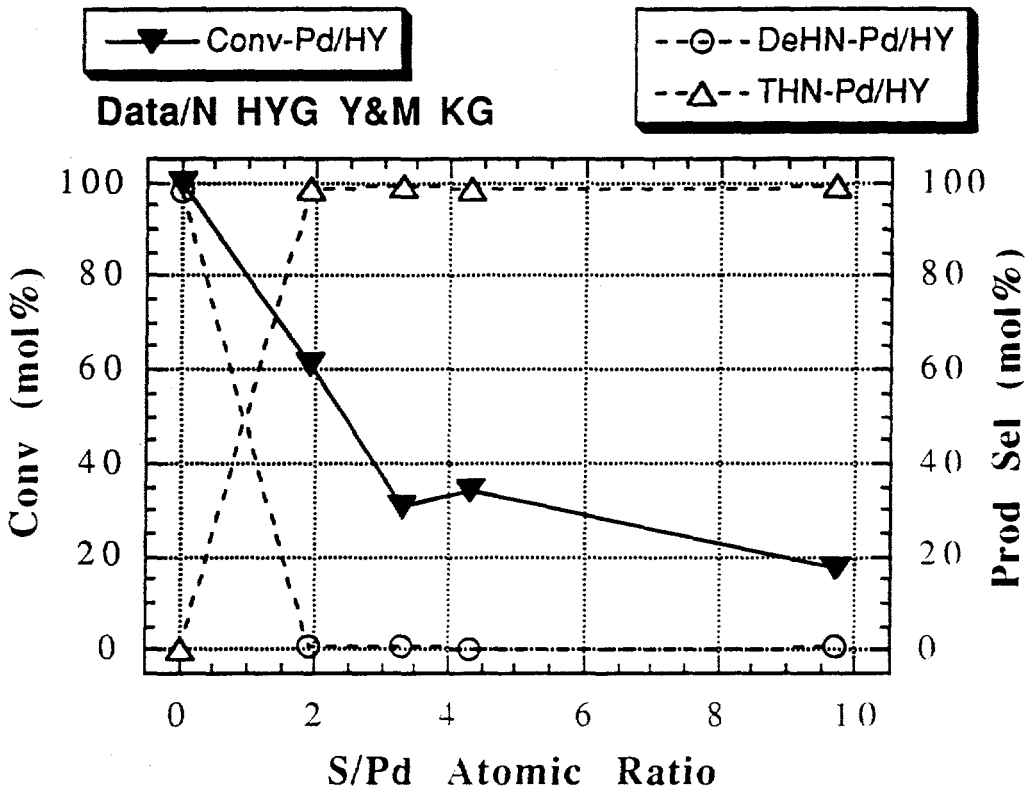

Figure 5. Effect of sulfur/Pd atomic ratio on naphthalene conversion and selectivity to tetralin and decahydronaphthalene over Pd/HY at 200°C in the presence of added benzothiophene.